

Supplemental Information

**MAU2 and NIPBL Variants Impair
the Heterodimerization of the Cohesin Loader
Subunits and Cause Cornelia de Lange Syndrome**

Ilaria Parenti, Farah Diab, Sara Ruiz Gil, Eskeatnaf Mulugeta, Valentina Casa, Riccardo Berutti, Rutger W.W. Brouwer, Valerie Dupé, Juliane Eckhold, Elisabeth Graf, Beatriz Puisac, Feliciano Ramos, Thomas Schwarzmayr, Macarena Moronta Gines, Thomas van Staveren, Wilfred F.J. van IJcken, Tim M. Strom, Juan Pié, Erwan Watrin, Frank J. Kaiser, and Kerstin S. Wendt

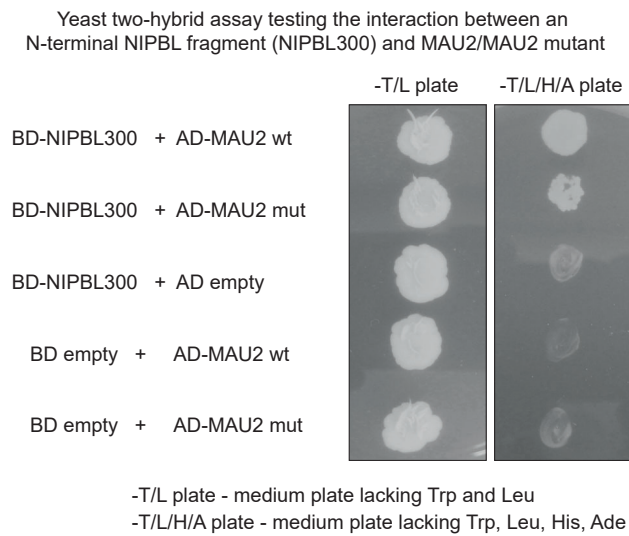


Figure S1: Related to Figure 1.

The in-frame deletion p.(Gln310_Ala316del) in MAU2 impairs its interaction with NIPBL

The yeast two-hybrid assay shows a slower growth of yeasts on selective medium in the presence of the MAU2 deletion, supporting the results obtained with the mammalian two-hybrid assay.

The left panel shows interaction-independent growth of yeasts on Trp- and Leu-deficient plates.

The right panel illustrates the interaction-dependent growth of yeasts expressing NIPBL and MAU2 in plates lacking Trp, Leu, His and Ade.

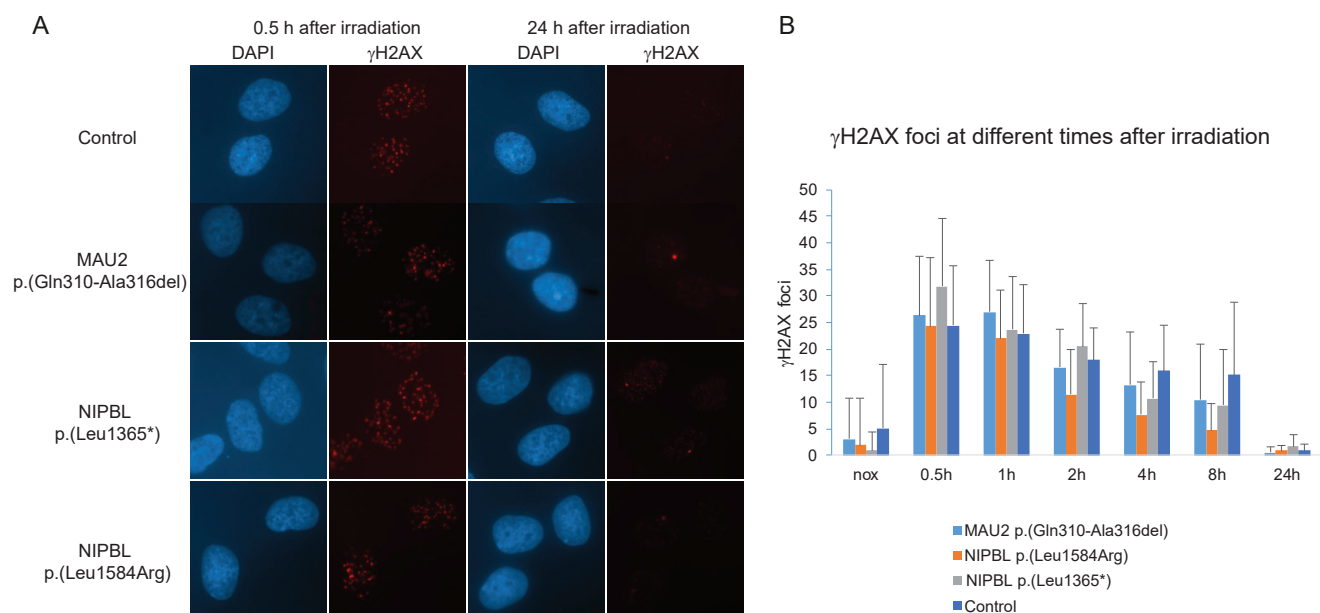


Figure S2: Related to Figure 1.

Response of CdLS fibroblast cells to DNA damage

A) Skin fibroblasts of a healthy control, from two patients with different NIPBL mutations (NIPBL p.Leu1365*, NIPBL p.Leu1584Arg) and from the patient with deletion in MAU2 (MAU2 p.Gln310-Ala 316del) were exposed to 1 Gy gamma-irradiation. DNA double strand breaks (DSB's) were visualized by immunostaining for γ H2AX at different time points after exposure.

B) To assess DSB repair, the number of DSBs at different time points was quantitated as number of γ H2AX foci. Data are presented as means from n=3 experiments \pm SEM.

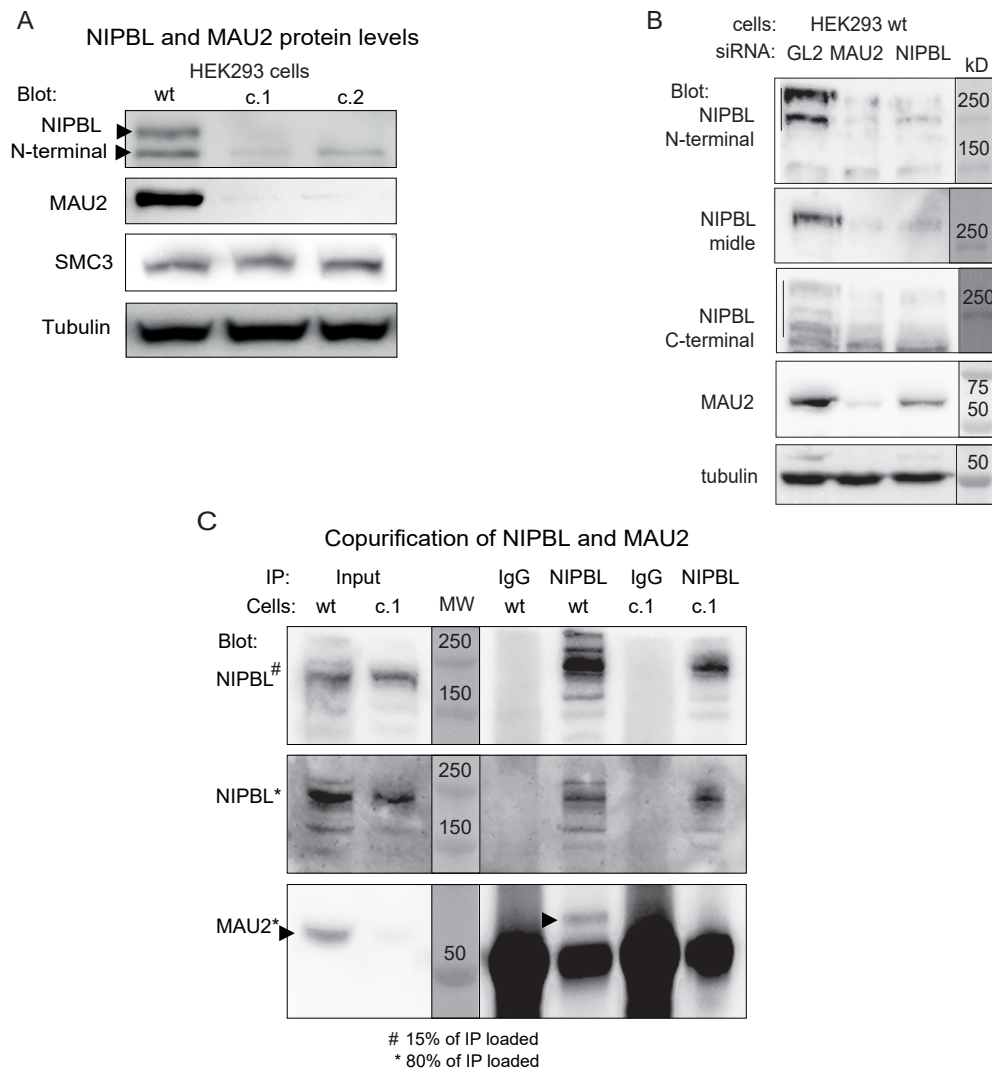


Figure S3: Related to Figure 3.

NIPBL and MAU2 depletion by siRNA knockdown and quantitation of MAU2 protein levels in NIPBLΔN cells

A) Western blots with total cell lysates from HEK293 NIPBLΔN cells, probed with antibodies against NIPBL, MAU2, SMC3 and tubulin.

B) Knockdown of MAU2 and NIPBL by siRNA in HEK293 cells. Total cell lysates were loaded and the blots probed with antibodies directed against the N-terminus and the C-terminus of NIPBL reveal which of the detected bands are NIPBL (marked with a line) and which are unspecific bands. Further, rabbit polyclonal antibodies raised against residues 744-977 from mouse Nipbl were used (NIPBL middle). Note that NIPBL depletion leads to a strong reduction of MAU2 protein levels and *vice versa*.

C) Immunoprecipitation (IP) of NIPBL from nuclear extracts of HEK293 wt and NIPBLΔN clone c.1 and detection of NIPBL and MAU2 by western blotting. NIPBL could be immunoprecipitated in wt and NIPBLΔN cells while MAU2 was only coprecipitated in wt cells, demonstrating that the residual MAU2 is unable to interact with NIPBLΔN. The strong signals in the anti-MAU2 immunoblot are caused by the IgGs used for immunoprecipitation. The arrowhead indicates MAU2. A similar blot for another HEK293 NIPBLΔN clone and for HT1080 cells is included in Figure 3D.

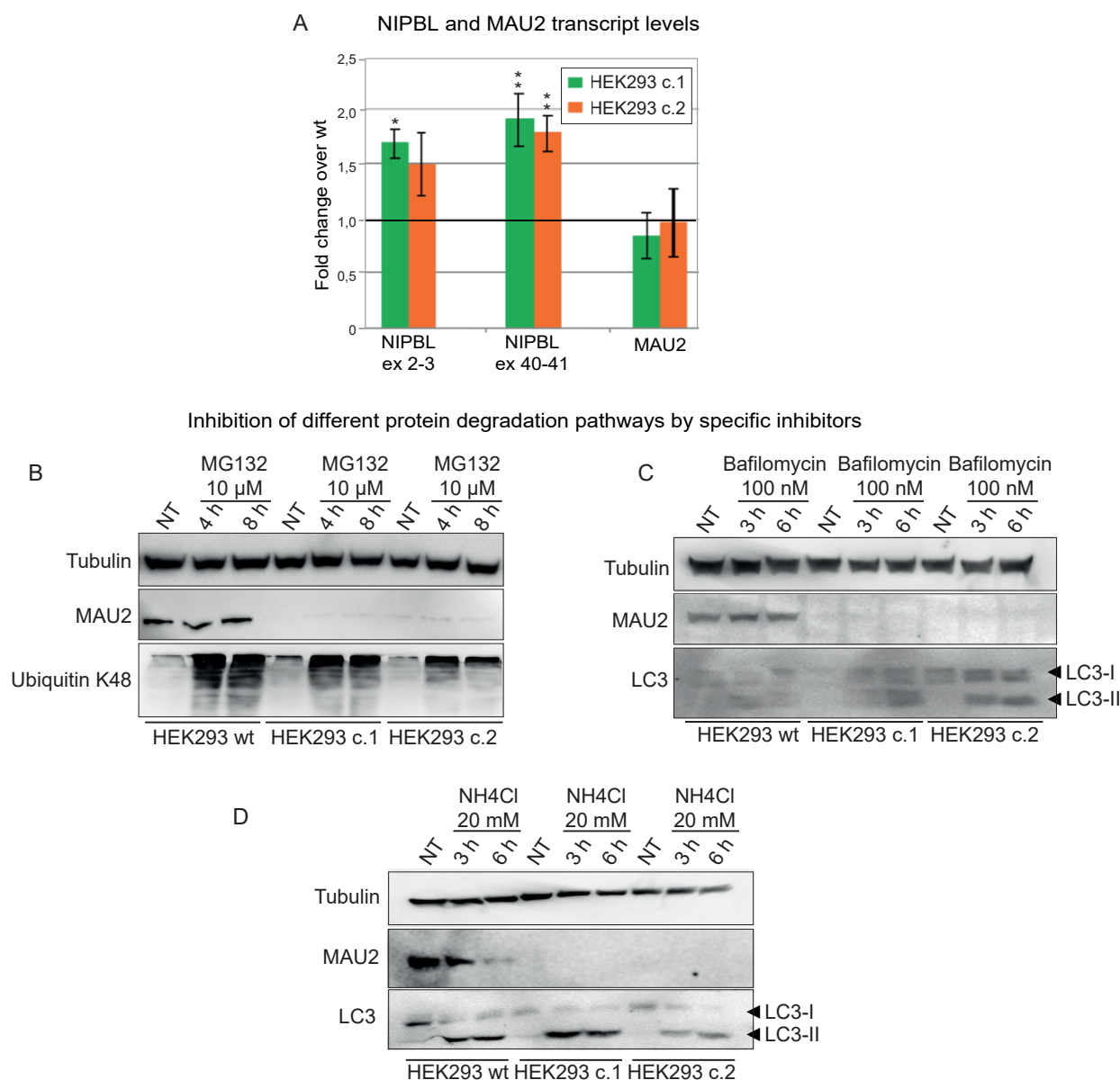


Figure S4: Related to Figure 3.

MAU2 loss does not depend on the main cellular protein degradation pathways

A) Analysis of NIPBL and MAU2 transcript levels. Expression data were normalized to GAPDH and relative mRNA levels compared to wt cells were determined using the $\Delta\Delta C_t$ method. MAU2 expression appears to be largely unchanged in NIPBL Δ N cells (Bilateral unpaired T-test; c1 $p=0.09$, c2 $p=0.85$), while two different intron-spanning primer pairs for NIPBL (ex 2-3 and ex 40-41) show increased NIPBL transcript levels (Bilateral unpaired T-test; exon 2-3: c1 $*p=0.03$, c2 $p=0.06$; exon 40-41: c1 $**p=0.006$, c2 $**p=0.001$).

B) MG132 treatment leads to the inhibition of the proteasome degradation pathway. Poly-ubiquitination of K48 was used as a positive control for the treatment (upon arrest of the proteasome with MG132, proteins with the ubiquitin degradation marker on K48 accumulate in the cell). Despite the success of the treatment with MG132, MAU2 expression could not be restored in the NIPBL Δ N cells, indicating that the proteasome is not responsible for MAU2 degradation.

C-D) Bafilomycin (inhibition of fusion between autophagosome and lysosome) (C) and Ammonium chloride (NH4Cl, alteration of lysosomal pH) (D) are both responsible for the arrest of the autophagy flux. The conversion of the soluble LC3-I to lipid-bound LC3-II is associated with the formation of autophagosomes. LC3-II associates with the membrane of the autophagosomes and is degraded after fusion of the autophagosome with the lysosome. When cells are treated with Ammonium chloride or Bafilomycin, the degradation of LC3-II is blocked, resulting in its accumulation. Upon treatment of the NIPBL Δ N cells with these two agents, LC3-II levels increased, whereas MAU2 expression could not be restored. Altogether, these results indicate that the autophagy flux is not responsible for the loss of MAU2.

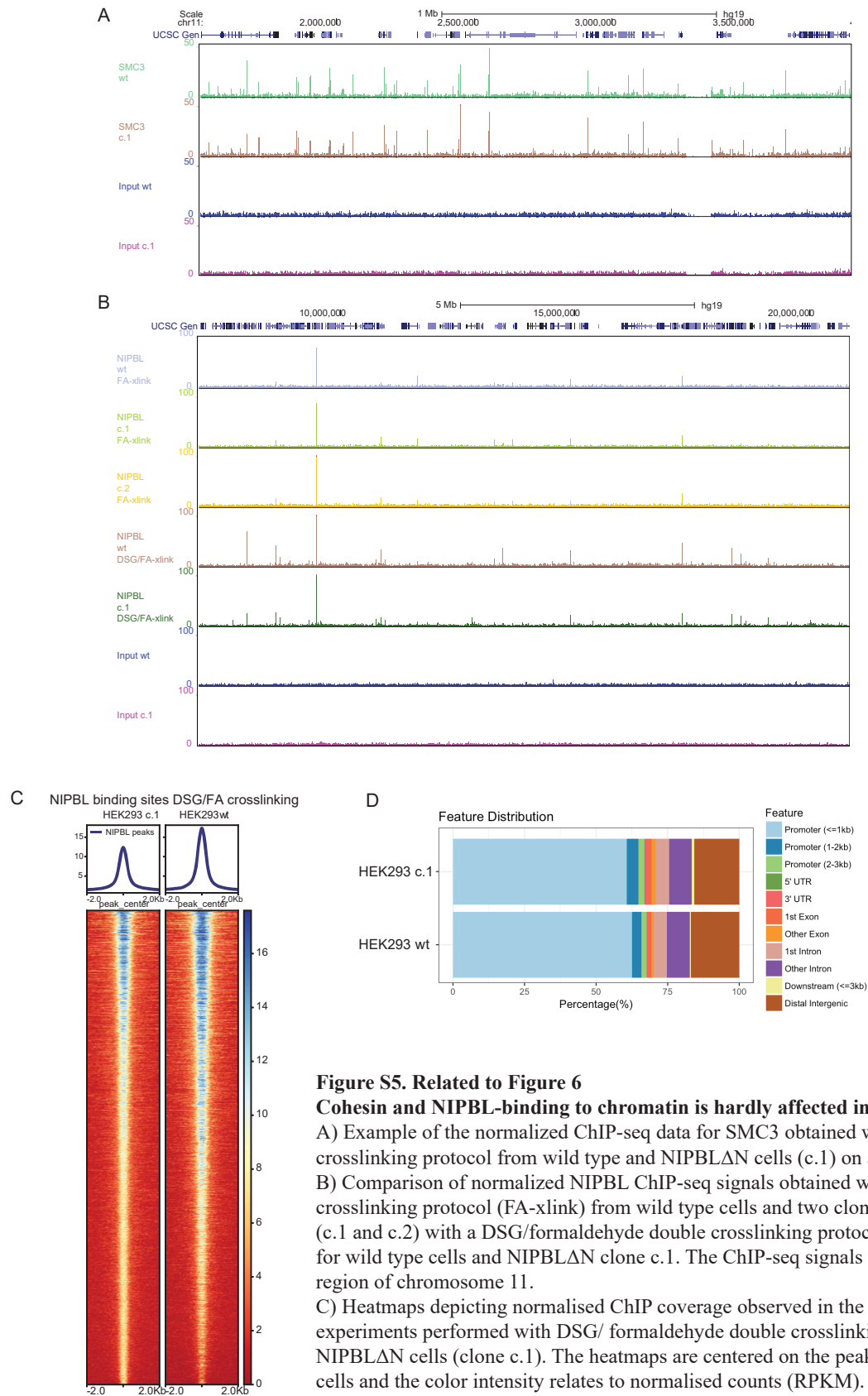


Figure S5. Related to Figure 6

Cohesin and NIPBL-binding to chromatin is hardly affected in NIPBLΔN cells

A) Example of the normalized ChIP-seq data for SMC3 obtained with a formaldehyde-crosslinking protocol from wild type and NIPBLΔN cells (c.1) on a region of chr11.

B) Comparison of normalized NIPBL ChIP-seq signals obtained with a formaldehyde-crosslinking protocol (FA-xlink) from wild type cells and two clones of NIPBLΔN cells (c.1 and c.2) with a DSG/formaldehyde double crosslinking protocol (DSG/FA-xlink) for wild type cells and NIPBLΔN clone c.1. The ChIP-seq signals displayed represent a region of chromosome 11.

C) Heatmaps depicting normalised ChIP coverage observed in the NIPBL ChIP-seq experiments performed with DSG/ formaldehyde double crosslinking for wild type and NIPBLΔN cells (clone c.1). The heatmaps are centered on the peaks observed in wild type cells and the color intensity relates to normalised counts (RPKM).

D) Distribution of the peaks observed in the SMC3 and NIPBL ChIP-seq experiments performed with a DSG/formaldehyde double crosslinking protocol (DSG/FA-xlink) over different genomic features (eg. promoters, introns, exons) for wild type and NIPBLΔN cells. No striking differences are visible between wild type and NIPBLΔN cells.

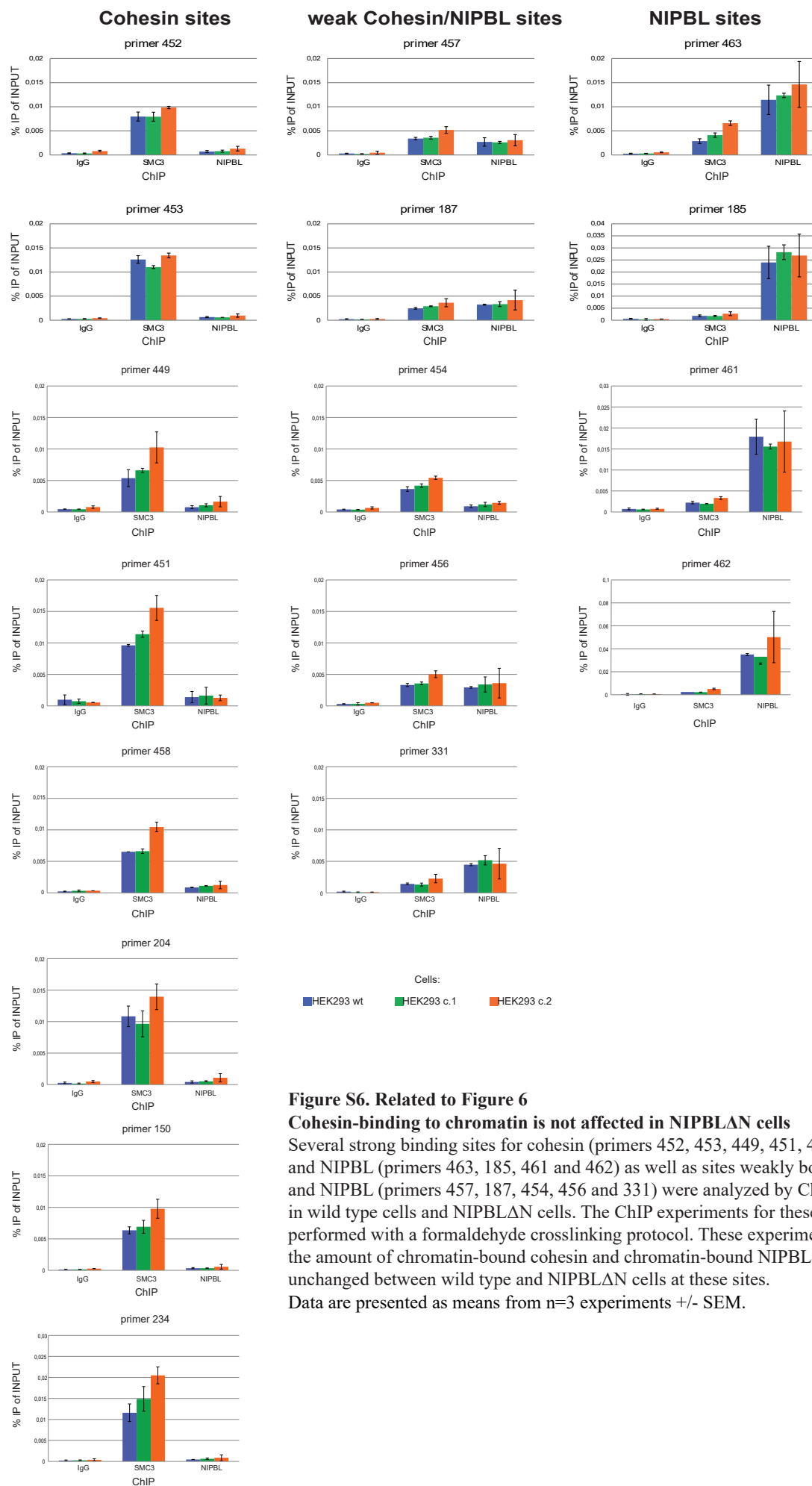


Figure S6. Related to Figure 6

Cohesin-binding to chromatin is not affected in NIPBLΔN cells

Several strong binding sites for cohesin (primers 452, 453, 449, 451, 458, 204, 150, 234) and NIPBL (primers 463, 185, 461 and 462) as well as sites weakly bound by cohesin and NIPBL (primers 457, 187, 454, 456 and 331) were analyzed by ChIP-qPCR in wild type cells and NIPBLΔN cells. The ChIP experiments for these samples were performed with a formaldehyde crosslinking protocol. These experiments indicate that the amount of chromatin-bound cohesin and chromatin-bound NIPBL is mainly unchanged between wild type and NIPBLΔN cells at these sites.

Data are presented as means from n=3 experiments +/- SEM.

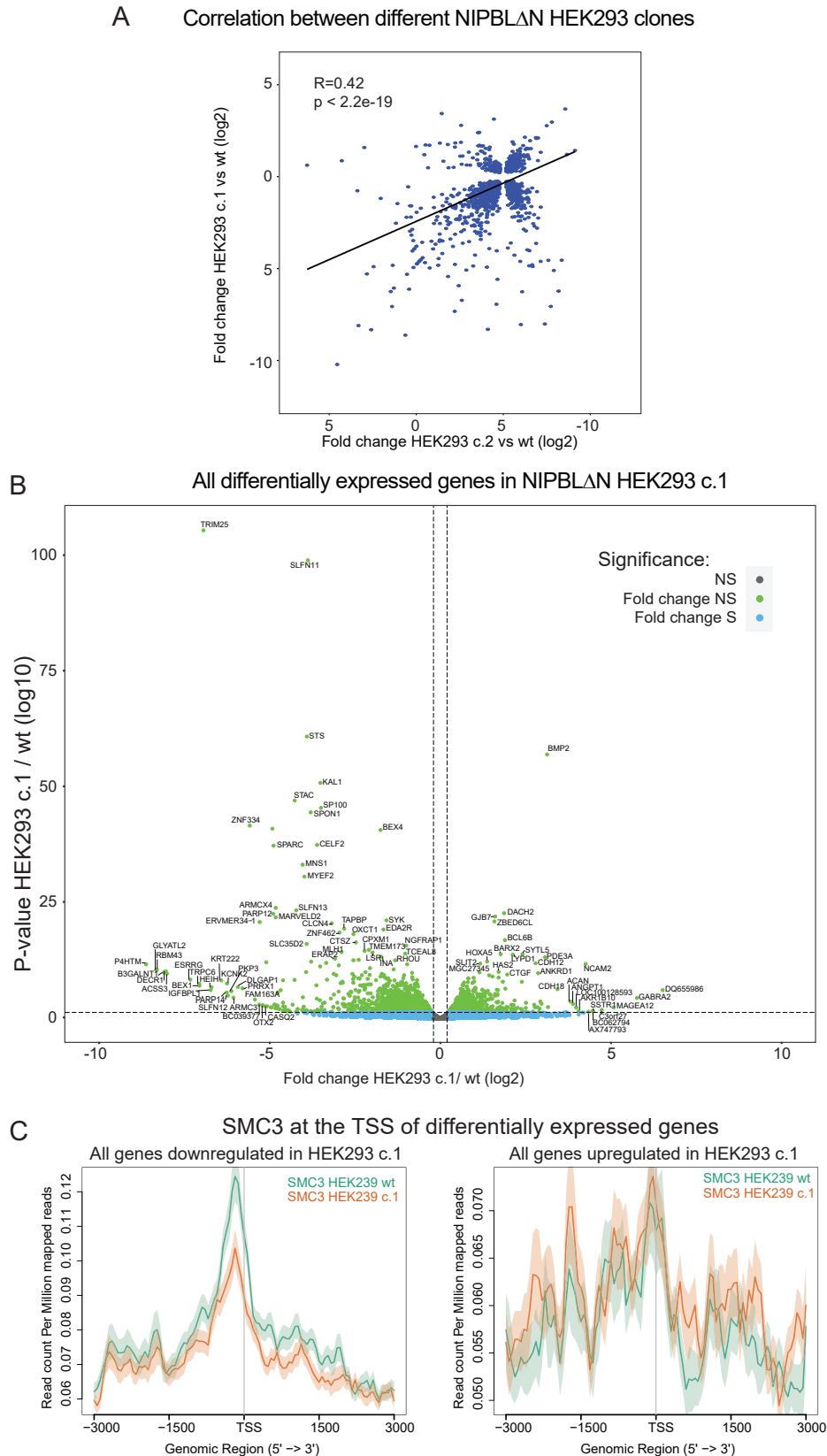


Figure S7. Related to Figure 6. Transcriptome analysis of NIPBLΔN HEK293 cells.

A) Scatter plot showing the correlation of the fold changes between two different HEK293 cell clones (HEK293 c.1 on the x-axis and HEK293 c.2 on the y-axis). The Pearson correlation coefficient (R) and the p-value (p) are shown in the graph.

B) Volcano plot showing the distribution of up and downregulated genes in H293 cells (HEK293c.1).

Genes with p-values < 0.05 are shown as blue dots, genes with a |FC| < 1 are shown as grey dots.

The green dots show genes with significant FC and P-values. Note that we show here the differentially expressed genes for the HEK293 c.1 clone. Genes that show inconsistent changes between the two analyzed clones c.1 and c.2 are not removed.

C) Plots showing the SMC3 coverage at promoters of genes downregulated or upregulated in NIPBLΔN cells

Table S1:

GO-term analysis of differentially expressed genes in MAU2 p.(Gln310-Ala316del) fibroblasts and NIPBL p.(Leu1365*) fibroblasts versus a healthy control, related to Figure 2

Analysis with Webgestalt (<http://www.webgestalt.org/>), genes with p-value <0.05 and FC outside [-1;+1] were included. The options term redundancy reduced by weighted set cover were used. Overlapping |GO-terms are highlighted in red.

MAU2p.(Gln310-Ala316del) fibroblasts versus healthy control fibroblasts

Gene Set	Description	Size	Expect	Ratio	P Value	FDR
GO:0008283	cell proliferation	1986	383.28	1.4532	0	0
GO:0006928	movement of cell or subcellular component	1967	379.61	1.5700	0	0
GO:0009888	tissue development	1925	371.51	1.5854	0	0
GO:2000026	regulation of multicellular organismal development	1908	368.23	1.6077	0	0
GO:0046903	secretion	1605	309.75	1.4237	0	0
GO:0048585	negative regulation of response to stimulus	1545	298.17	1.4723	0	0
GO:0022610	biological adhesion	1377	265.75	1.7611	0	0
GO:1902531	regulation of intracellular signal transduction	1824	352.02	1.3721	1.1102e-15	1.2616e-13
GO:0006468	protein phosphorylation	1860	358.96	1.3567	7.5495e-15	7.7115e-13
GO:0006811	ion transport	1608	310.33	1.3856	1.1102e-14	1.0853e-12

NIPBL p.L1365* fibroblasts versus healthy control fibroblasts

Gene Set	Description	Size	Expect	Ratio	P Value	FDR
GO:0006928	movement of cell or subcellular component	1967	165.37	1.6327	0	0
GO:0009888	tissue development	1925	161.84	1.7363	0	0
GO:2000026	regulation of multicellular organismal development	1908	160.41	1.8328	0	0
GO:0022610	biological adhesion	1377	115.77	1.9954	0	0
GO:0007267	cell-cell signaling	1575	132.42	1.6916	3.3307e-16	1.4419e-13
GO:0008283	cell proliferation	1986	166.97	1.5991	4.4409e-16	1.8351e-13
GO:0010647	positive regulation of cell communication	1732	145.62	1.6276	3.7748e-15	1.2256e-12
GO:0046903	secretion	1605	134.94	1.6007	4.6496e-13	8.4539e-11
GO:0051049	regulation of transport	1765	148.39	1.5567	1.1726e-12	1.9382e-10
GO:1901700	response to oxygen-containing compound	1556	130.82	1.5747	8.6525e-12	1.1918e-9

Table S2 - related to Figure S5

qPCR primer for the analysis of ChIP samples

primer	forward	reverse	genomic coordinates (hg19)
150	GGCTCAGGACAGAAGTGACC	AGGTCGGCAGAGGCTCC	chr22:32925080-32925266
204	TTCAGCCGGTTCAAGGGACG	CTAGGGAGGAGGACAGAGGCAAGAG	chr11:2058315-2058501
234	AATGACGGAGCTGCGAGATAC	TTGCTAGGCAACCTGACAGAC	chr5:43313810-43313992
331	AGGTGGCACTGTTGCATAG	CCTGCCAAAGGAGAGCTTTATC	chr11:1630677-1630849
449	AGATGAAGCACAGGTGGTGAAC	CAACACCGACTGCTTGAAATCC	chr11:20359017-20359262
451	CCTGGCAATTTACGGTGTAGG	ATAAGCCGCACTAGAAGGACCC	chr22:37252291-37252540
452	TTCGGAAGAGGCAGGGAAG	GTGGCAGCACCCAAGTTAG	chr22:38259504-38259680
454	GAGTCTTTCCTTGCCTCTTC	GGGAGCCCATAAATGTCAC	chr5:36935893-36936139
456	TTCCCAGAGCCCAGAATACAAG	GTAGCGCGAAATAAGGATTCCG	chr19:4246755-4246932
457	GACAGGCCACGTTATTGAC	ACCCTCCAGCAAGACAGAAG	chr19:7,694,524-7,694,677
458	CCGACCACAAGGACGGATTC	CCGCTCTCAGCTTCCTCTTC	chr19:8008922-8009140
461	CCGCCCACCTAACCTTTATTC	AGTTGCGAGGCAGAGTTTG	chr9:130829458-130830053
462	AAAGCAGAGGGCGACTTAGG	TCAGGAAGCTGTAGCGAGAG	chr9:139780556-139781018
463	GCCGAGCAGCATTGACCAAC	TCTCGGCTGGGCTCTACTTC	chr3:88107986-88108569

Table S5: GO-term analysis of differentially expressed genes in NIPBLΔN HEK293, related to Figure 6 and Figure S7

Biological pathways from DEGs in HEK (common DEGs, $|FC| > 1$, $p < 0.05$), reduction of redundancy by weighted set cover (<http://www.webgestalt.org/>).

Gene Set	Description	Size	Expect	Ratio	P Value	FDR
GO:0051240	positive regulation of multicellular organismal process	1661	19.736	2.2801	9.5321e-8	0.00067473
GO:0040011	locomotion	1738	20.651	2.0822	0.0000022940	0.0013903
GO:0040007	growth	961	11.419	2.5397	0.0000034190	0.0016660
GO:0007610	behavior	582	6.9153	3.0368	0.0000061493	0.0021925
GO:2000026	regulation of multicellular organismal development	1908	22.671	1.9408	0.000010588	0.0029167
GO:0032989	cellular component morphogenesis	1082	12.856	2.3335	0.000012112	0.0029760
GO:0042493	response to drug	994	11.811	2.3707	0.000018391	0.0035138
GO:0043062	extracellular structure organization	400	4.7528	3.3665	0.000024087	0.0042936
GO:0007267	cell-cell signaling	1575	18.714	1.9771	0.000042091	0.0061043
GO:0009611	response to wounding	642	7.6282	2.6219	0.000082512	0.0092607

Table 6 ChIP-sequencing statistics, related to STAR methods

Sample ID	Sample	Cell line	sequenced reads	genome
I17-1066-01	SMC3 ChIP	HEK293 wt	26066918	hg19
I17-1066-02	NIPBL ChIP	HEK293 wt	23349918	hg19
I17-1066-04	Input	HEK293 wt	20655989	hg19
I17-1066-05	SMC3 ChIP	HEK293 c.1	20269237	hg19
I17-1066-06	NIPBL ChIP	HEK293 c.1	20505412	hg19
I17-1066-08	Input	HEK293 c.1	24265890	hg19
I17-1284-01	SMC3 ChIP	HEK293 wt	24250592	hg19
I17-1284-02	SMC3 ChIP	HEK293 c.1	25637885	hg19
I17-1310-01	SMC3 ChIP	HEK293 wt	26517943	hg19
I17-1310-02	SMC3 ChIP	HEK293 wt	30302933	hg19
I17-1310-03	Input	HEK293 wt	27249816	hg19
I17-1310-04	SMC3 ChIP	HEK293 c.1	30785668	hg19
I17-1310-05	NIPBL ChIP	HEK293 c.1	32568589	hg19
I17-1310-06	Input	HEK293 c.1	25557021	hg19
I17-1310-07	SMC3 ChIP	HEK293 c.2	30369459	hg19
I17-1310-08	NIPBL ChIP	HEK293 c.2	29778688	hg19
I17-1310-09	Input	HEK293 c.2	23724637	hg19
I17-1066-03	NIPBL ChIP (Beth	HEK293 wt	24539800	hg19
I17-1066-07	NIPBL ChIP (Beth	HEK293 c.1	23793483	hg19

Table S7 RNA-sequencing statistics, related to STAR methods

Sample ID	Cell line	sequenced reads	genome	mapped reads		unmapped reads	
				read number	percent	read number	percent
LUEB0120	Control fibroblasts	99439773	hg19	97203044	97,75%	2236729	2,25%
LUEB0129	Control fibroblasts	81304856	hg19	78691729	96,79%	2613127	3,21%
LUEB0130	Control fibroblasts	74240231	hg19	72118457	97,14%	2121774	2,86%
LUEB0123	NIPBL mut fibroblasts	77501979	hg19	75245221	97,09%	2256758	2,91%
LUEB0124	NIPBL mut fibroblasts	81246927	hg19	78853528	97,05%	2393399	2,95%
LUEB0125	NIPBL mut fibroblasts	75030331	hg19	73602333	98,10%	1427998	1,90%
LUEB0126	MAU2 mut fibroblasts	78344410	hg19	76627687	97,81%	1716723	2,19%
LUEB0127	MAU2 mut fibroblasts	97053241	hg19	95405627	98,30%	1647614	1,70%
LUEB0128	MAU2 mut fibroblasts	77196493	hg19	75583417	97,91%	1613076	2,09%
LUEB0157	Control HEK293 cells	111677363	hg19	109161179	97,75%	2516184	2,25%
LUEB0158	Control HEK293 cells	99089929	hg19	95208004	96,08%	3881925	3,92%
LUEB0159	Control HEK293 cells	98830348	hg19	96576515	97,72%	2253833	2,28%
LUEB0160	CRISPR/Cas9 HEK293 c.10 cells	97689690	hg19	93721355	95,94%	3968335	4,06%
LUEB0161	CRISPR/Cas9 HEK293 c.10 cells	93990390	hg19	88485178	94,14%	5505212	5,86%
LUEB0162	CRISPR/Cas9 HEK293 c.10 cells	92127803	hg19	87747608	95,25%	4380195	4,75%
LUEB0163	CRISPR/Cas9 HEK293 c.2.1 cells	100406239	hg19	94761904	94,38%	5644335	5,62%
LUEB0164	CRISPR/Cas9 HEK293 c.2.1 cells	107339878	hg19	98971476	92,20%	8368402	7,80%
LUEB0165	CRISPR/Cas9 HEK293 c.2.1 cells	100408584	hg19	95803500	95,41%	4605084	4,59%